

# CODE-CL: Conceptor-Based Gradient Projection for Deep Continual Learning

Marco P. E. Apolinario   Sakshi Choudhary   Kaushik Roy  
Elmore Family School of Electrical and Computer Engineering  
Purdue University, West Lafayette, IN 47906

mapolina@purdue.edu, choudh23@purdue.edu, kaushik@purdue.edu

## Abstract

*Continual learning (CL) – the ability to progressively acquire and integrate new concepts – is essential to intelligent systems to adapt to dynamic environments. However, deep neural networks struggle with catastrophic forgetting (CF) when learning tasks sequentially, as training for new tasks often overwrites previously learned knowledge. To address this, recent approaches constrain updates to orthogonal subspaces using gradient projection, effectively preserving important gradient directions for previous tasks. While effective in reducing forgetting, these approaches inadvertently hinder forward knowledge transfer (FWT), particularly when tasks are highly correlated. In this work, we propose Conceptor-based gradient projection for Deep Continual Learning (CODE-CL), a novel method that leverages conceptor matrix representations, a form of regularized reconstruction, to adaptively handle highly correlated tasks. CODE-CL mitigates CF by projecting gradients onto pseudo-orthogonal subspaces of previous task feature spaces while simultaneously promoting FWT. It achieves this by learning a linear combination of shared basis directions, allowing efficient balance between stability and plasticity and transfer of knowledge between overlapping input feature representations. Extensive experiments on continual learning benchmarks validate CODE-CL’s efficacy, demonstrating superior performance, reduced forgetting, and improved FWT as compared to state-of-the-art methods.<sup>1</sup>*

## 1. Introduction

Humans possess the innate ability to continually acquire, retain and update knowledge to adapt naturally to dynamically changing environments. In contrast, while deep neural networks (DNNs) excel at leveraging massive amounts of data to generalize across various visual recognition tasks, traditional learning paradigms rely on static datasets. This misalignment with the ever-evolving real-world environ-

ments underscores the necessity for these models to retain past knowledge and mitigate catastrophic forgetting, as well as utilize it to enhance learning on new tasks by encouraging knowledge transfer [6, 9, 12, 28].

To address the challenges mentioned above, extensive research has focused on enabling continual learning (CL) in DNNs. Existing techniques fall into three categories: regularization-based, expansion-based, and memory-based methods. Regularization-based methods constrain updates to important model parameters for previous tasks, preserving essential features while allowing flexibility in less critical regions of the parameter space [10, 17, 25, 26, 35]. Expansion-based methods overcome forgetting by dynamically allocating new network resources for each task [18, 21, 30, 32, 33]. Memory-based approaches, on the other hand, store representative samples for data replay or track important gradient directions from previous tasks to maintain performance on earlier data distributions [2, 3, 5, 16, 19, 23, 29, 34]. While these techniques significantly reduce catastrophic forgetting, they inherently limit the model’s ability to leverage shared information across tasks. In other words, they help retain past task performance, but have limited ability to utilize prior knowledge to improve learning on new tasks. Recent works have attempted to enhance knowledge transfer in continual learning scenarios by leveraging task similarities to integrate past knowledge into new learning [14, 15, 22]. However, we demonstrate that they do not fully incorporate a systematic approach, leaving room for further improvements.

In this paper, we propose Conceptor-Based Gradient Projection (CODE-CL), a novel continual learning algorithm that minimizes catastrophic forgetting while promoting forward knowledge transfer between tasks with highly correlated input activation subspaces. CODE-CL leverages conceptor matrices [8] to enforce constrained gradient updates, preventing interference with prior tasks. More precisely, conceptor matrices provide a mathematical framework for computing the basis vectors of each layer’s input activation/feature space, which, in turn, identify the key gradient directions necessary to retain knowledge from past

<sup>1</sup>Our code is available at <https://github.com/mapolinario94/CODE-CL>

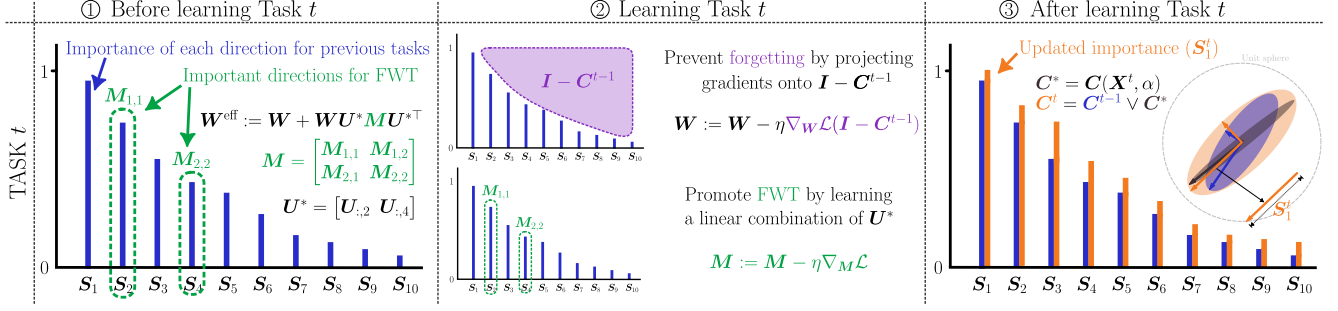


Figure 1. Overview of CODE-CL. ① Before learning task  $t$ , the importance of input activation space directions for previous tasks is captured in the singular values  $S_i^{t-1}$  (blue bars) of the conceptor matrix  $C^{t-1}$ . We first identify  $U^*$ , the important directions for both previous tasks and the current task  $t$ . If such shared directions exist, we define  $W^{\text{eff}}$  by projecting weights onto a linear combination of these common directions:  $W^{\text{eff}} = W + WU^*MU^{*\top}$ . ② During the learning phase, CODE-CL promotes forward knowledge transfer (FWT) by learning an optimal linear combination of the directions ( $M$ ), while preventing forgetting by projecting gradients onto  $I - C^{t-1}$  (purple region). This ensures that the updates do not interfere with the previously acquired knowledge. ③ After learning task  $t$ , the updated importance of each direction ( $S_i^t$ ) is computed by obtaining a new conceptor matrix:  $C^t = C^{t-1} \vee C^*$ , where  $C^*$  is the conceptor matrix for task  $t$ . Since a conceptor matrix can be interpreted as an ellipsoid in space, where its singular vectors ( $U$ ) define main axes and its singular values ( $S$ ) determine their lengths, operation  $\vee$  corresponds to computing the minimal enclosing ellipsoid that encapsulates both conceptors. In this manner, CODE-CL enables efficient continual learning by balancing knowledge retention and adaptation to new tasks.

tasks [36]. We also compute similarities between previously acquired knowledge and the new incoming task to optimize forward transfer (FWT). By encoding past knowledge into conceptor matrices, CODE-CL enables a structured exploration of the input activation space, allowing learning in previously restricted regions while preserving critical directions from earlier tasks. We give an overview of our approach in Fig. 1. At the end of each task, CODE-CL computes a set of basis vectors,  $U$ , that span the input feature space and consequently, the gradient space for each layer using the conceptor matrix  $C$  [22, 23, 36]. For a new task, gradient updates are projected in these directions  $U$ , scaled according to their importance for previous tasks with a regularization factor  $\alpha$ . While this constrained optimization effectively mitigates catastrophic forgetting, it does not explicitly promote forward knowledge transfer. To address this, we compute the intersection between the aggregated conceptor matrix and the pre-conceptor matrix of the current task, identifying common update directions  $U^*$  and encouraging learning along these directions through  $M$ , as shown in Fig. 1.

Our contributions can be summarized as follows:

- We introduce CODE-CL, a novel continual learning algorithm that leverages conceptor matrices [8] to mitigate catastrophic forgetting while effectively leveraging past learning to promote forward transfer.
- We evaluate the effectiveness of the proposed method through extensive experiments on standard CL vision benchmarks across various model architectures. Compared to state-of-the-art approaches, CODE-CL achieves about 1.15% better final accuracy, minimal forgetting,

and up to 1.18% improved relative FWT.

## 2. Background

In this section, we outline the essential properties of conceptor matrices, and provide an overview of related works in continual learning.

### 2.1. Conceptor Matrices

Conceptor matrices constitute a mathematical framework inspired by neuroscience to encode and control the dynamics of recurrent neural networks [8]. Given a batch of feature vectors  $X \in \mathbb{R}^{b \times n}$ , where  $b$  is the batch size and  $n$  is the dimension of the feature vector space, a conceptor matrix  $C(X, \alpha)$  is defined as the solution to the following minimization problem:

$$C(X, \alpha) = \arg \min_C \frac{1}{b} \|X - XC\|_F^2 + \alpha^{-2} \|C\|_F^2 \quad (1)$$

Here,  $\alpha \in (0, \infty)$  is called the aperture and serves as a regularization factor. This optimization problem has the following closed-form solution [8]:

$$C(X, \alpha) = \frac{X^\top X}{b} \left( \frac{X^\top X}{b} + \alpha^{-2} I \right)^{-1} \quad (2)$$

Therefore, given the singular value decomposition (SVD) of the matrix  $X^\top X = U \Sigma V^\top$ , the conceptor matrix can be expressed as  $C = U S U^\top = U \Sigma^2 (\Sigma^2 + b \alpha^{-2} I)^{-1} U^\top$ . Note, the singular values of  $C$  lie between 0 and 1 ( $0 < S_{i,i} < 1, \forall i \in \{0, 1, \dots, n\}$ ), representing the importance

of directions  $U_{:,i}$ . In this way,  $C$  acts as a soft projection matrix onto the linear subspace of the feature vectors of  $X$ .

Conceptor matrices satisfy most laws of Boolean logic like NOT ( $\neg$ ), OR ( $\vee$ ), and AND ( $\wedge$ ) [8], resulting in a simple and intuitive framework to handle the linear subspaces defined within a conceptor matrix. For two conceptor matrices  $C$  and  $B$ , we have:

$$\neg C = I - C \quad (3)$$

$$C \wedge B = (C^{-1} + B^{-1} - I)^{-1} \quad (4)$$

$$C \vee B = \neg(\neg C \wedge \neg B) \quad (5)$$

Here,  $\neg C$  can be interpreted as the pseudo-orthogonal complement of the subspace characterized by  $C$ .  $C \wedge B$  signifies the conceptor matrix that describes a space that lies in the intersection between the subspaces characterized by  $C$  and  $B$ , and  $C \vee B$  describes the union between the subspaces represented by  $C$  and  $B$ . Please refer to Section A in the Supplementary Material for additional details regarding these operations.

We can measure the capacity, or memory usage, of a conceptor matrix based on the mean value of its singular values:

$$\Theta(C) = \frac{1}{n} \sum_{i=0}^n S_{i,i} \quad (6)$$

A capacity of 0 would indicate that the conceptor is empty and can be represented as a null matrix, while a capacity of 1 would indicate that the conceptor memory is full, essentially becoming an identity matrix.

## 2.2. Related Work

Continual learning (CL) techniques can be broadly classified into expansion-based, regularization-based, and memory-based approaches [14, 23, 28].

Regularization-based methods mitigate forgetting by penalizing changes to important model parameters [10, 17, 20, 24, 25, 35]. While effective at preserving knowledge, these methods often rely on complex heuristics to determine parameter importance or require storing multiple model versions, leading to significant memory overhead.

Expansion-based methods address catastrophic forgetting by dynamically increasing the model’s capacity as new tasks arrive [18, 21, 30, 32]. Although these approaches successfully isolate task representations to prevent interference, they result in substantial network growth, making them impractical for resource-constrained environments.

Memory-based methods mitigate forgetting by explicitly retaining information from previous tasks, either in the form of stored samples [2, 19] or gradient-related information [3, 16]. Within this category, orthogonal gradient projection methods [7, 23, 34] aim to prevent interference between tasks by ensuring that the gradients are orthogonal

to important directions for previous tasks. One such approach is Gradient Projection Memory (GPM) [23], which leverages the fact that gradients lie in the span of input activations [36]. Consequently, GPM utilizes singular value decomposition (SVD) on the input activations of each layer to compute and store the most important directions for each task. While this prevents forgetting, it also limits forward knowledge transfer (FWT) by keeping the shared directions between old and new tasks frozen, reducing adaptability and degrading accuracy.

Trust Region Gradient Projection (TRGP) [14] addresses this by selectively allowing weight updates in a “trusted region”. Specifically, TRGP computes the projection of new task gradients onto the important directions of previous tasks and identifies the top- $k$  tasks with the highest projections. Weight updates are then allowed along the directions associated with these  $k$  tasks. However, this approach still lacks fine-grained adaptability, as it considers entire task subspaces rather than individual relevant directions. Building on TRGP, Continual Learning with Backward Knowledge Transfer (CUBER) [15] introduces positive backward transfer (BWT) by maintaining per-task gradient information. If a new task’s gradients exhibit a positive correlation with those of the previous tasks, CUBER relaxes the orthogonality constraint and introduces a regularization term to the loss function to align updates along these correlated directions. While this promotes positive BWT, it significantly increases memory complexity due to the need to store per-task gradients. Scaled Gradient Projection (SGP) [22] takes a different approach by relaxing the strict orthogonality constraint of GPM. Instead of enforcing full orthogonality, SGP scales the importance of stored task directions, leading to better forward knowledge transfer (FWT) and higher average accuracy. However, SGP applies uniform scaling across all tasks, missing opportunities to adaptively exploit task similarities. Other notable methods include Adaptive Plasticity Improvement (API), which combines GPM’s gradient constraints with dynamic model expansion when plasticity is insufficient, and Space Decoupling (SD) [37], which scales gradient projections based on task correlation, allowing for a more flexible gradient update strategy compared to TRGP and GPM. Taking a different perspective, Data Augmented Flatness-aware Gradient Projection (DFGP) [31] extends GPM by optimizing the loss as well as loss curvature from the perspective of both data and weights. This improves the generalization ability for new tasks and reduces catastrophic forgetting for the past tasks. However, DFGP does not explicitly leverage task similarities to facilitate knowledge transfer.

In contrast to the aforementioned works, CODE-CL constrains gradients to pseudo-orthogonal directions through a regularized reconstruction framework based on conceptor matrices, as shown in (2). Additionally, we perform a

fine-grained analysis to identify the common important directions between tasks. Our proposed approach not only mitigates catastrophic forgetting but also enhances FWT by intelligently reusing prior knowledge.

### 3. Methodology

#### 3.1. Problem Formulation

This work optimizes a DNN model to learn from temporally evolving data. We consider a supervised continual learning setting where  $T$  tasks are learned sequentially, with each task having sufficient labeled samples. We explore task-incremental learning scenarios in this supervised setting [28]. Each task is identified by  $t \in \mathbb{T} = \{1, 2, \dots, T\}$ , and its associated dataset is represented as  $\mathbb{D}^t = \{(\mathbf{x}_i^t, y_i^t)_{i=1}^{n_t}\}$ , where  $n_t$  is the number of samples,  $\mathbf{x}_i^t$  is the input sample, and  $y_i^t$  is the corresponding label. Using these datasets, we train a neural network with parameters  $\mathbb{W}^t = \{(\mathbf{W}^{(l),t})_{l=1}^L\}$ , where  $L$  represents the number of layers of the model. The objective is to learn parameters  $\mathbb{W}^t$  such that the model performs effectively across all  $T$  tasks, while mitigating catastrophic forgetting and leveraging task similarities for efficient knowledge transfer.

#### 3.2. Approach

We demonstrate the flow of our proposed approach, CODE-CL in Algorithm 1. For the first task ( $t = 1$ ), learning proceeds with random weight initialization and the model is trained on dataset  $\mathbb{D}^1$  by minimizing the loss function  $\mathcal{L}(\mathbf{W}; \mathbb{D}^1)$ . Optimization is performed using minibatch stochastic gradient descent (SGD) without constraints. After training for  $E$  epochs, we compute a conceptor matrix  $\mathbf{C}^1$  to encode the input subspace of each layer (lines 21-23, Algorithm 1). Specifically, we randomly sample  $b$  inputs from  $\mathbb{D}^1$  and perform a forward pass through the model to form  $\mathbf{X}^1 = [\mathbf{x}_1^{1\top}, \mathbf{x}_2^{1\top}, \dots, \mathbf{x}_b^{1\top}]$  for each layer  $l$ , i.e.  $\mathbb{X}^1 = \{(\mathbf{X}^{(l),1})_{l=1}^L\}$ . Based on (2), we compute the conceptor  $\mathbf{C}^1 = \mathcal{C}(\mathbf{X}^1, \alpha)$ .

##### 3.2.1. Task Overlap Analysis

Before training for the task  $t$ , we analyze the overlap between its input space and that of previous tasks, represented by  $\mathbf{C}^{t-1}$ . To do this, we forward propagate a set of inputs  $\mathbf{X}^t$  through the model, obtain layer-wise input activations  $\mathbb{X}^t$  and compute the pre-conceptor matrix  $\mathbf{C}^{t,\text{pre}}$  through equation (2) (lines 3-4, Algorithm 1). The overlap of the input space between previous tasks and the current task  $t$  is represented by the intersection  $\mathbf{C}^{t,\text{and}} = \mathbf{C}^{t,\text{pre}} \wedge \mathbf{C}^{t-1}$ , based on (4). If many directions for the current task are encoded in  $\mathbf{C}^{t-1}$ , tasks are highly correlated (or similar). Task correlation is measured by the capacity ratio between conceptor matrices (6), defining high (low) correlation when the ratio surpasses (falls below) a threshold  $\epsilon$ .

---

#### Algorithm 1 CODE-CL

---

**Input:**  $\mathbb{D}^t = \{(\mathbf{x}_i^t, y_i^t)_{i=1}^{n_t}\}$ ,  $\mathbb{W} = \{(\mathbf{W}^{(l)})_{l=1}^L\}$ , aperture  $\alpha$ , threshold  $\epsilon$ , learning rate  $\eta$ , total training epochs  $E$ , number of free dimensions  $K$ .

##### procedure TRAIN()

```

1.  for  $t = 1, 2, 3, \dots, T$ 
2.    if  $t > 1$  then
3.       $\mathbb{X}^t \leftarrow \text{forward}(\mathbb{W}^{t-1,\text{eff}}, d^t)$  for  $d^t \sim \mathbb{D}^t$ 
4.       $\mathbf{C}^{t,\text{pre}} \leftarrow \text{CONCEPTOR}(\mathbb{X}^t, \alpha)$ 
5.       $\mathbf{C}^{t,\text{and}} \leftarrow \mathbf{C}^{t,\text{pre}} \wedge \mathbf{C}^{t-1}$   $\triangleright$  Equation (4)
6.      if  $\frac{\Theta(\mathbf{C}^{t,\text{and}})}{\Theta(\mathbf{C}^{t-1})} > \epsilon$  then  $\triangleright$  for each layer  $l \in L$ 
7.         $\mathbf{U}^t \leftarrow \text{SVD}(\mathbf{C}^{t,\text{and}})$ 
8.         $\mathbf{W}^{t,\text{eff}} \leftarrow \mathbf{W}(\mathbf{I} + \mathbf{U}_{:,1:K}^t \mathbf{M}^t \mathbf{U}_{:,1:K}^{t\top})$ 
9.      else
10.        $\mathbf{W}^{t,\text{eff}} \leftarrow \mathbf{W}$ 
11.    end
12.  end
13.  end
14.   $\mathbb{W}^{t,\text{eff}} \leftarrow \{(\mathbf{W}^{t,\text{eff}})_{l=1}^L\}$ 
15.  for  $e = 1, 2, 3, \dots, E$ 
16.     $\nabla_{\mathbb{W}} \mathcal{L}, \nabla_{\mathbf{M}^t} \mathcal{L} \leftarrow \text{SGD}(\mathbb{W}^{t,\text{eff}}, d^t)$  for  $d^t \sim \mathbb{D}^t$ 
17.     $\nabla_{\mathbb{W}} \mathcal{L} \leftarrow \nabla_{\mathbb{W}} \mathcal{L} - \nabla_{\mathbb{W}} \mathcal{L} \mathbf{C}^{t-1}$   $\triangleright$  for each layer  $l$ 
18.     $\mathbb{W} \leftarrow \mathbb{W} - \eta \nabla_{\mathbb{W}} \mathcal{L}$ 
19.     $\mathbf{M}^t \leftarrow \mathbf{M}^t - \eta \nabla_{\mathbf{M}^t} \mathcal{L}$ 
20.  end
21.   $\mathbb{X}^t \leftarrow \text{forward}(\mathbb{W}, d^t)$  for  $d^t \sim \mathbb{D}^t$ 
22.   $\mathbf{C}^{t,\text{post}} \leftarrow \text{CONCEPTOR}(\mathbb{X}^t, \alpha)$ 
23.  if  $t = 1$  then
24.     $\mathbf{C}^t \leftarrow \mathbf{C}^{t,\text{post}}$ 
25.  else
26.     $\mathbf{C}^t \leftarrow \mathbf{C}^{t,\text{post}} \vee \mathbf{C}^{t-1}$   $\triangleright$  Equation (5)
27.  end
```

---

**Case 1** ( $\frac{\Theta(\mathbf{C}^{t,\text{and}})}{\Theta(\mathbf{C}^{t-1})} > \epsilon$ ): In this high correlation scenario, the directions encoded in  $\mathbf{C}^{t-1}$  are important for task  $t$ . Hence, the model is allowed to learn in the top  $K$  directions of  $\mathbf{C}^{t,\text{and}}$  without negatively impacting prior tasks. To achieve this, the weights are projected onto the subspace defined by these directions as follows:

$$\mathbf{W}^{t,\text{eff}} = \mathbf{W} + \mathbf{W} \mathbf{U}_{:,1:K}^{t,\text{and}} \mathbf{M}^t \mathbf{U}_{:,1:K}^{t,\text{and}\top}, \quad (7)$$

where  $\mathbf{U}_{:,1:K}^{t,\text{and}}$  are the top- $K$  singular vectors of  $\mathbf{C}^{t,\text{and}}$ , and  $\mathbf{M} \in \mathbb{R}^{K \times K}$  is a task-specific learnable matrix which defines the extent of learning in these directions. This formulation explicitly allows us to utilize past knowledge to improve the performance of the current task, thereby improving forward knowledge transfer.

**Case 2** ( $\frac{\Theta(\mathbf{C}^{t,\text{and}})}{\Theta(\mathbf{C}^{t-1})} \leq \epsilon$ ): In this case, the task overlap is minimal, leaving little possibility of forward transfer. Thus, the effective weights remain  $\mathbf{W}^{t,\text{eff}} = \mathbf{W}$ .



### 3.2.2. Constrained Gradient Updates

While learning task  $t$ , the model is trained on  $\mathbb{D}^t$  to minimize the following loss function:

$$\begin{aligned} \mathbf{W}^t, \mathbf{M}^t &:= \arg \min_{\mathbf{W}, \mathbf{M}} \mathcal{L}(\mathbf{W}^{t,\text{eff}}; \mathbb{D}^t) \\ \text{s.t. } \nabla_{\mathbf{W}} \mathcal{L} &= \nabla_{\mathbf{W}} \mathcal{L}(\mathbf{I} - \mathbf{C}^{t-1}), \end{aligned} \quad (8)$$

where the gradients are constrained to lie in the pseudo-orthogonal subspace of the conceptor matrix defined by  $-\mathbf{C}^{t-1}$  (3), where  $\mathbf{C}^{t-1}$  contains important directions for previous tasks, scaled by aperture  $\alpha$ , as shown in (2).

### 3.2.3. Post Training Conceptor Update

After training for task  $t$ , we merge the current and past task knowledge into a new conceptor matrix  $\mathbf{C}^t$  for each layer (line 26, Algorithm 1). This is achieved by first computing the post-training conceptor matrix  $\mathbf{C}^{t,\text{post}}$ , as shown in lines 21-22 in Algorithm 1. We then merge  $\mathbf{C}^{t,\text{post}}$  and  $\mathbf{C}^{t-1}$  into a new conceptor matrix, consolidating the important directions for all learned tasks based on (5).

## 4. Experiments

In this section, we first provide details regarding our experimental setup, and then show the efficacy of CODE-CL through extensive experiments across various continual learning benchmarks.

### 4.1. Experimental Setup

In this subsection, we outline the benchmarks, network architectures, training hyperparameters, and performance metrics used to evaluate and compare our method with state-of-the-art CL techniques.

#### 4.1.1. Benchmarks and Models

We evaluate our method on widely used continual learning (CL) benchmarks, including Split CIFAR100 [11], Split miniImageNet [27], and 5-Datasets [4]. For Split CIFAR100, the original CIFAR100 dataset is divided into  $T$  groups, each containing an equal number of classes ( $100/T$ ). In our experiments, we split the dataset into 10 groups, with each group representing a separate task, and train a 5-layer AlexNet model in a multi-head setting, where each head is associated with one unique task [14, 22, 23]. Similarly, the Split miniImageNet benchmark consists of a subset of 100 classes from the ImageNet dataset, divided into 20 groups. The 5-Datasets benchmark involves training a model sequentially on five different datasets: CIFAR10, MNIST, SVHN, notMNIST, and Fashion MNIST. For both Split miniImageNet and 5-Datasets, we use a reduced ResNet18 model in a multi-head setting [14, 22, 23]. To ensure a fair comparison with prior works, we refrain from using data augmentation in our experiments. The dataloaders for Split CIFAR100 and 5-Datasets are obtained

from GPM[23], while the one for Split miniImageNet was provided by the Avalanche library [1].

#### 4.1.2. Training Details

For all our experiments, we use stochastic gradient descent (SGD) with a learning rate scheduler and early stopping criteria [23]. Each task in Split CIFAR100 is trained for a maximum of 200 epochs with a batch size of 64 and aperture  $\alpha = 6$ . Similarly, each task in Split miniImageNet and 5-Datasets is trained for a maximum of 100 epochs with a batch size of 64, and with  $\alpha = 16$  and  $\alpha = 8$ , respectively. For all our experiments as shown in Table 1, we use  $K = 80$ . For more details on our implementation, please refer to Section C in the Supplementary Material.

#### 4.1.3. Performance Metrics

Similar to previous works [14, 16, 22, 23], we use three metrics to evaluate the performance of our method: the average final accuracy over all tasks, Accuracy (ACC), Backward Transfer (BWT), which measures the forgetting of old tasks when learning new tasks, and relative Forward Transfer (FWT), which measures the beneficial effects of learning the previous tasks for learning a new one. ACC and BWT are defined as:

$$\text{ACC} = \sum_{i=1}^T \frac{A_{T,i}}{T}; \text{BWT} = \sum_{i=1}^{T-1} \frac{A_{T,i} - A_{i,i}}{T-1}, \quad (9)$$

where  $T$  is the number of tasks,  $A_{j,i}$  is the accuracy of the model on  $i$ -th task after learning the  $j$ -th task sequentially ( $i \leq j$ ). Similarly, FWT is defined as:

$$\text{FWT} = \frac{1}{T} \sum_{i=1}^T A_{i,i} - B_{i,i}, \quad (10)$$

where  $B_{i,i}$  is the accuracy of a baseline method used for training the same model on the  $i$ -th task. In our experiments, we used GPM [23] as the baseline to compare other methods.

## 4.2. Results

Here, we present the performance of CODE-CL in comparison with prior approaches, along with a detailed analysis of its memory complexity. Additionally, we conduct ablation studies to assess the impact of varying the number of free dimensions,  $K$ , on the method’s performance.

### 4.2.1. Performance Comparison

As shown in Table 1, our method achieves high accuracy with minimal forgetting across all benchmarks. Specifically, CODE-CL consistently delivers competitive results, outperforming previous methods on all three datasets.

In terms of accuracy, on Split CIFAR100, CODE-CL achieves 77.21%, coming close to the upper bound set

Table 1. Performance comparison on continual image classification datasets using multi-head networks. Accuracy and BWT (mean  $\pm$  std) are reported over five trials. Best results are in bold and second best are underlined.  $^\dagger$  denotes the results taken from [23] and  $^\ddagger$  denote the results from the respective original papers. All other results are reproduced based on their official open source implementations.

Method	Split CIFAR100		Split MiniImageNet		5-Datasets	
	ACC (%)	BWT (%)	ACC (%)	BWT (%)	ACC (%)	BWT (%)
Multitask $^\dagger$	79.58 $\pm$ 0.54	—	69.46 $\pm$ 0.62	—	91.54 $\pm$ 0.28	—
OWM [34] $^\dagger$	50.94 $\pm$ 0.60	-30 $\pm$ 1	—	—	—	—
EWC [10] $^\dagger$	68.80 $\pm$ 0.88	-2 $\pm$ 1	52.01 $\pm$ 2.53	-12 $\pm$ 3	88.64 $\pm$ 0.26	-4 $\pm$ 1
HAT [25] $^\dagger$	72.06 $\pm$ 0.50	0 $\pm$ 0	59.78 $\pm$ 0.57	-3 $\pm$ 0	91.32 $\pm$ 0.18	-1 $\pm$ 0
A-GEM [3] $^\dagger$	63.98 $\pm$ 1.22	-15 $\pm$ 2	57.24 $\pm$ 0.72	-12 $\pm$ 1	84.04 $\pm$ 0.33	-12 $\pm$ 1
ER_Res [2] $^\dagger$	71.73 $\pm$ 0.63	-6 $\pm$ 1	58.94 $\pm$ 0.85	-7 $\pm$ 1	80.31 $\pm$ 0.22	-4 $\pm$ 0
API [13] $^\ddagger$	—	—	65.9 $\pm$ 0.6	-0.3 $\pm$ 0.2	91.1 $\pm$ 0.3	-0.5 $\pm$ 0.1
DFGP [31] $^\ddagger$	74.59 $\pm$ 0.33	-0.9	69.92 $\pm$ 0.9	-1	92.09 $\pm$ 0.18	-1
TRGP+SD [37] $^\ddagger$	75.50 $\pm$ 0.35	-2.88 $\pm$ 0.89	65.8 $\pm$ 0.16	-0.49 $\pm$ 0.08	—	—
GPM [23]	72.06 $\pm$ 0.29	-0.2 $\pm$ 0.19	66.26 $\pm$ 1.18	-0.9 $\pm$ 1.34	90.70 $\pm$ 0.45	-1.0 $\pm$ 0.16
TRGP [14]	75.24 $\pm$ 0.29	-0.1 $\pm$ 0.18	65.08 $\pm$ 0.94	-0.5 $\pm$ 0.74	<u>92.81 <math>\pm</math> 0.54</u>	-0.1 $\pm$ 0.03
CUBER [15]	75.30 $\pm$ 0.43	0.1 $\pm$ 0.11	64.25 $\pm$ 0.75	-0.7 $\pm$ 0.48	<u>92.77 <math>\pm</math> 0.60</u>	-0.03 $\pm$ 0.02
SGP [22]	<u>75.69 <math>\pm</math> 0.38</u>	-1.4 $\pm$ 0.17	68.50 $\pm$ 2.09	-2.0 $\pm$ 2.10	90.42 $\pm$ 0.66	-1.61 $\pm$ 0.31
CODE-CL (Ours)	<b>77.21 <math>\pm</math> 0.32</b>	-1.1 $\pm$ 0.28	<b>71.16 <math>\pm</math> 0.32</b>	-1.1 $\pm$ 0.3	<b>93.51 <math>\pm</math> 0.13</b>	-0.11 $\pm$ 0.01

Table 2. Comparison of relative FWT with respect to GPM [23]. Values (mean  $\pm$  std) are reported over five trials. Best results are in bold and second best are underlined.

Method	S-CIFAR100	S-MiniImageNet	5-Datasets
	FWT (%)	FWT (%)	FWT (%)
TRGP [14]	2.86 $\pm$ 0.26	-1.56 $\pm$ 0.67	<u>1.16 <math>\pm</math> 0.52</u>
CUBER [15]	2.86 $\pm$ 0.49	-2.22 $\pm$ 0.70	1.10 $\pm$ 0.60
SGP [22]	<u>4.74 <math>\pm</math> 0.37</u>	<u>3.37 <math>\pm</math> 0.88</u>	0.33 $\pm$ 0.37
CODE-CL	<b>5.92 <math>\pm</math> 0.34</b>	<b>4.17 <math>\pm</math> 0.41</b>	<b>1.82 <math>\pm</math> 0.12</b>

by Multitask Learning (79.58%), which serves as an ideal but unrealistic comparison point. Notably, CODE-CL outperforms other state-of-the-art continual learning methods, achieving higher accuracy than all previous approaches, including API, DFGP, TRGP+SD, GPM, TRGP, CUBER, and SGP. Similarly, on Split MiniImageNet and 5-Datasets, CODE-CL once again performs exceptionally well, surpassing all other previous methods. In both cases, it even exceeds the accuracy of the Multitask Learning baseline, illustrating the beneficial effect of forward knowledge transfer when learning tasks sequentially. This further underscores CODE-CL’s robustness, particularly on more challenging datasets, where competing methods tend to suffer significant performance drops.

Fig. 2 presents the model’s accuracy for each task immediately after learning it ( $A_{i,i}$ ) and after sequentially learning all tasks ( $A_{T,i}$ ) in the Split CIFAR100 dataset. The difference between these two measures quantifies the extent of forgetting. As shown, CODE-CL achieves superior  $A_{i,i}$

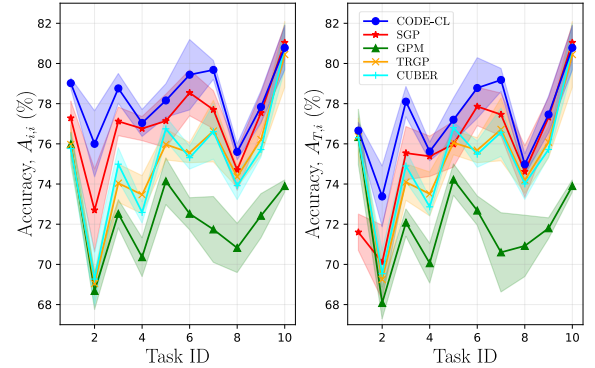


Figure 2. Test accuracy of each task on the Split CIFAR100 benchmark: (left) immediately after learning the task,  $A_{i,i}$ ; (right) after learning all tasks,  $A_{T,i}$ . Here, it can be seen that our method outperforms previous methods for all tasks.

and  $A_{T,i}$  compared to other methods across all tasks. This advantage arises mainly because, unlike methods such as GPM, TRGP, or CUBER, CODE-CL incorporates pseudo-orthogonal gradient projections. Additionally, in contrast to SGP, our method enables the selective release of important shared directions, further enhancing forward transfer.

To quantify this, we measure the relative FWT of key representative methods (TRGP, CUBER, and SGP) and compare them against CODE-CL using GPM as a reference. The results, presented in Table 2, demonstrate that CODE-CL consistently achieves better FWT. This can be attributed to its relaxation of gradient projections into pseudo-orthogonal spaces, unlike TRGP or CUBER, and

Table 3. Memory complexity comparison among methods. The analysis is done for a single fully-connected layer with  $N$  inputs,  $M$  outputs, after being trained on  $T$  tasks. Also,  $B$  is the average number of important direction per task used in [14] and  $K$  is the number of free dimensions parameter used in CODE-CL.

Methods	GPM	TRGP	CUBER	SGP	CODE-CL (Ours)
Memory Complexity	$O(N^2)$	$O(N^2 + TNB + TB^2)$	$O(N^2 + TN^2 + TNB + TB^2)$	$O(N^2)$	$O(N^2 + TNK + TK^2)$

its fine-grained selection of the most important shared directions among tasks, unlike the other methods.

In terms of BWT, our results further illustrate CODE-CL’s effectiveness in mitigating catastrophic forgetting. On Split CIFAR100, CODE-CL records a BWT of -1.1%, indicating minimal performance loss on previously learned tasks, comparable to prior works. Similarly, on Split Mini-ImageNet, CODE-CL achieves a BWT of -1.1%, aligning with state-of-the-art methods and demonstrating its ability to retain learned knowledge with minimal degradation. Finally, on the 5-Datasets benchmark, CODE-CL reports a BWT of -0.11%, performing similarly to TRGP.

In summary, the high accuracy, low forgetting, and improved FWT of CODE-CL highlight its ability to effectively balance the trade-off between plasticity and stability, maintaining strong performance across a range of continual learning tasks while minimizing forgetting.

#### 4.2.2. Memory Complexity

We analyze the memory complexity of our proposed approach and compare it with state-of-the-art techniques GPM, SGP, TRGP and CUBER. For simplicity, we analyze a single fully connected layer with  $N$  inputs and  $M$  outputs after training on  $T$  tasks. CODE-CL’s memory complexity is primarily influenced by conceptor matrices of size  $N^2$ , which encode input vector space information. Additionally, as discussed in Section 3, CODE-CL allocates a fixed number of free dimensions per task ( $K$ ) to learn an optimal linear combination of the  $K$  most important directions within the subspace formed by the intersection of past and new task conceptors. This introduces an additional memory requirement of  $TNK + TK^2$ , where  $TNK$  accounts for the storage of  $K$  key directions per task of dimension  $N$ , and  $TK^2$  accounts for learnable square matrices  $M^t$ . Consequently, the total memory complexity of CODE-CL is  $O(N^2 + TNK + TK^2)$ .

For GPM and SGP, memory usage is determined solely by the input dimension  $N$ , leading to a  $O(N^2)$  complexity. TRGP shares this base complexity but also stores important directions per task and trusted region projection subspaces, incurring an additional cost of  $O(TNB + TB^2)$ , where  $B$  is the number of important directions per task. Similarly, CUBER requires  $O(N^2 + TN^2 + TNB + TB^2)$ , with the additional  $TN^2$  term arising from additional gradient storage needs.

Table 3 summarizes the memory complexity of each

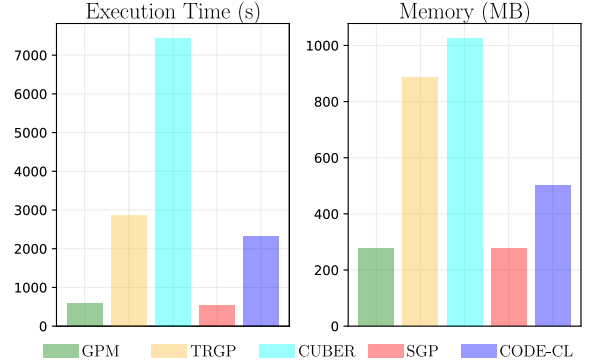


Figure 3. Execution time (left) and memory (right) comparison on the Split CIFAR100 benchmark. Lower means better. Here, CODE-CL represent a more efficient method than techniques such as TRGP or CUBER.

method. In particular, as model size (i.e.  $N$ ) grows, CODE-CL maintains a fixed and significantly smaller number of free dimensions ( $K \ll N$ ), making its memory requirements comparable to GPM, SGP, and TRGP, while being significantly lower than CUBER. GPU memory usage measurements on Split CIFAR100 (Fig. 3) confirm CODE-CL’s efficiency, requiring half the memory of TRGP and CUBER. Additionally, CODE-CL achieves a slightly shorter execution time than TRGP and is approximately  $3\times$  faster than CUBER. While it introduces some overhead compared to GPM and SGP, this trade-off is justified by its superior performance.

#### 4.2.3. Ablation Study

In this section, we examine the impact of the number of free dimensions ( $K$ ) and the aperture parameter ( $\alpha$ ) on performance. Note that we modify only one parameter at a time, keeping all other training hyperparameters fixed.

**Effects  $\alpha$  in performance:** As shown in Fig. 4,  $\alpha$  directly influences the model’s forgetting rate. Specifically, higher values of  $\alpha$  bring BWT closer to zero, meaning the model forgets less. This behavior aligns with the definition of conceptor matrices, as  $\alpha$  scales the singular values of the data. When  $\alpha \rightarrow \infty$ , the conceptor matrices approximate the identity matrix, preventing forgetting entirely. However, this also means that the model loses plasticity and is unable to integrate new information. This trade-off is evident in

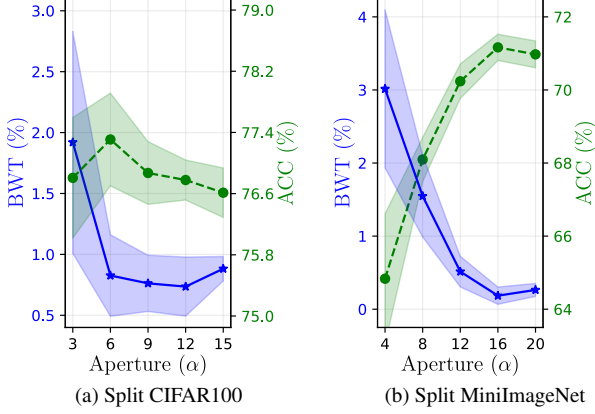


Figure 4. Effect of the aperture ( $\alpha$ ) parameter on ACC and BWT for the Split CIFAR-100 and Split miniImageNet benchmarks. In both cases, results show that the greater the  $\alpha$  ( $\uparrow$ ) parameter, the lower the BWT ( $\downarrow$ ), meaning the model forgets less.

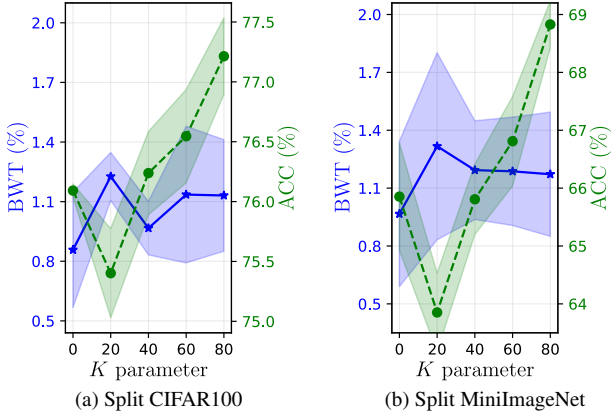


Figure 5. Effect of the number of free dimensions ( $K$ ) on the final accuracy and BWT for the Split CIFAR-100 and Split miniImageNet benchmarks. In both cases, results show that for  $K > 20$ , the greater the  $K$  ( $\uparrow$ ), the greater the ACC ( $\uparrow$ ), while BWT does not change significantly with  $K$ .

Fig. 4: for Split CIFAR100, peak performance is achieved at  $\alpha = 6$ , whereas for Split MiniImageNet, the optimal value is  $\alpha = 16$ .

**Effects  $K$  in performance:** The results for both benchmarks, presented in Fig. 5, indicate that increasing  $K$  generally improves accuracy while maintaining low BWT. When  $K > 20$ , higher values of  $K$  lead to greater ACC, suggesting that increasing  $K$  enhances overall performance by facilitating forward knowledge transfer from previous tasks to new ones. However, its impact on BWT reduction remains minimal. While increasing  $K$  may seem advantageous, it comes with additional memory overhead, making it crucial to balance performance gains with memory efficiency.

#### 4.2.4. Comparison on Tasks with Overlapping Classes

Most of the benchmarks used in this study consist of tasks with non-overlapping classes, although they share similarities in the feature space, as reflected in neuronal activity representations. While these benchmarks effectively demonstrate CODE-CL’s ability to identify the most relevant directions in overlapping feature spaces, evaluating our method on a benchmark with overlapping classes can further highlight its advantages. To this end, we adopted the OL-CIFAR100 benchmark [15], where the first 50 classes of CIFAR100 are split into seven tasks. Specifically, Tasks 0–6 contain the following class distributions: 0–9, 5–14, 10–19, 20–29, 25–34, 30–39, and 40–49, respectively.

The results of this evaluation are summarized in Table 4. Here, CODE-CL outperforms previous methods in terms of ACC, demonstrating the benefits of our approach in scenarios with class overlap. Additionally, we compute the relative FWT with respect to GPM. The superior FWT of CODE-CL underscores the effectiveness of our fine-grained selection of important directions within overlapping input feature subspaces. This, combined with pseudo-orthogonal gradient updates, leads to more efficient forward transfer learning compared to methods like TRGP or CUBER, which rely on full task directions, or SGP, which only considers pseudo-orthogonal gradient updates.

Table 4. Comparison of methods performance on OL-CIFAR100. Values (mean  $\pm$  std) are reported over five trials. Best results are in bold and second best are underlined.

Method	ACC (%)	BWT (%)	FWT (%)
GPM [23]	71.62 $\pm$ 0.45	-0.34 $\pm$ 0.15	0
TRGP [14]	74.77 $\pm$ 0.43	-0.06 $\pm$ 0.10	2.73 $\pm$ 0.34
CUBER [15]	75.01 $\pm$ 0.23	-0.01 $\pm$ 0.26	3.02 $\pm$ 0.20
SGP [22]	75.00 $\pm$ 0.68	-1.75 $\pm$ 0.59	<u>4.79 <math>\pm</math> 0.42</u>
CODE-CL	<b>76.89 <math>\pm</math> 0.42</b>	-1.01 $\pm$ 0.18	<b>6.02 <math>\pm</math> 0.36</b>

## 5. Conclusion

We introduce CODE-CL, a novel continual learning algorithm that leverages concept matrices to mitigate catastrophic forgetting while enhancing forward transfer. CODE-CL achieves this by projecting gradients onto pseudo-orthogonal subspaces of previous task feature spaces and learning a linear combination of shared basis directions. This approach effectively balances stability and plasticity, allowing efficient knowledge transfer across overlapping feature representations. Extensive experiments on standard continual learning benchmarks demonstrate CODE-CL’s effectiveness, achieving superior accuracy, minimal forgetting, and improved forward transfer compared to state-of-the-art methods.



## Acknowledgments

This work was supported in part by the Center for Co-design of Cognitive Systems (CoCoSys), one of the seven centers in JUMP 2.0, a Semiconductor Research Corporation (SRC) program, and in part by the Department of Energy (DoE).

## References

- [1] Antonio Carta, Lorenzo Pellegrini, Andrea Cossu, Hamed Hemati, and Vincenzo Lomonaco. Avalanche: A PyTorch Library for Deep Continual Learning. *Journal of Machine Learning Research*, 24(363):1–6, 2023. 5
- [2] Arslan Chaudhry, Marcus Rohrbach Facebook, A I Research, Mohamed Elhoseiny, Thalaiyasingam Ajanthan, Puneet K Dokania, Philip H S Torr, and Marc ' Aurelio Ranzato. On Tiny Episodic Memories in Continual Learning. *arXiv:1902.10486*, 2019. 1, 3, 6
- [3] Arslan Chaudhry, Marc ' Aurelio Ranzato, Marcus Rohrbach, and Mohamed Elhoseiny. Efficient Lifelong Learning with A-GEM. *International Conference on Learning Representations*, 2019. 1, 3, 6
- [4] Sayna Ebrahimi, Franziska Meier, Roberto Calandra, Trevor Darrell, and Marcus Rohrbach. Adversarial Continual Learning. In *Computer Vision – ECCV 2020: 16th European Conference, Glasgow, UK, August 23–28, 2020, Proceedings, Part XI*, pages 386–402, Berlin, Heidelberg, 2020. Springer-Verlag. 5
- [5] Mehrdad Farajtabar, Navid Azizan, Alex Mott, Ang Li, Deepmind Caltech, and Deepmind Deepmind. Orthogonal Gradient Descent for Continual Learning. In *Proceedings of the Twenty Third International Conference on Artificial Intelligence and Statistics*, pages 3762–3773. PMLR, 2020. 1
- [6] Raia Hadsell, Dushyant Rao, Andrei A. Rusu, and Razvan Pascanu. Embracing Change: Continual Learning in Deep Neural Networks. *Trends in Cognitive Sciences*, 24(12): 1028–1040, 2020. 1
- [7] Xu He and H. Jaeger. Overcoming Catastrophic Interference using Conceptor-Aided Backpropagation. *International Conference on Learning Representations*, 2018. 3
- [8] Herbert Jaeger. Controlling Recurrent Neural Networks by Conceptors. *arXiv:1403.3369*, 2014. 1, 2, 3
- [9] Zixuan Ke, Bing Liu, Nianzu Ma, Hu Xu, and Lei Shu. Achieving forgetting prevention and knowledge transfer in continual learning. In *Proceedings of the 35th International Conference on Neural Information Processing Systems*, Red Hook, NY, USA, 2021. Curran Associates Inc. 1
- [10] James Kirkpatrick, Razvan Pascanu, Neil Rabinowitz, Joel Veness, Guillaume Desjardins, Andrei A. Rusu, Kieran Milan, John Quan, Tiago Ramalho, Agnieszka Grabska-Barwinska, Demis Hassabis, Claudia Clopath, Dharshan Kumaran, and Raia Hadsell. Overcoming catastrophic forgetting in neural networks. *Proceedings of the National Academy of Sciences of the United States of America*, 114(13):3521–3526, 2017. 1, 3, 6
- [11] Alex Krizhevsky. Learning Multiple Layers of Features from Tiny Images. 2009. 5
- [12] Dhireesha Kudithipudi, Mario Aguilar-Simon, Jonathan Babb, Maxim Bazhenov, Douglas Blackiston, Josh Bongard, Andrew P. Brna, Suraj Chakravarthi Raja, Nick Cheney, Jeff Clune, Anurag Daram, Stefano Fusi, Peter Helfer, Leslie Kay, Nicholas Ketz, Zsolt Kira, Soheil Kolouri, Jeffrey L. Krichmar, Sam Kriegman, Michael Levin, Sandeep Madireddy, Santosh Manicka, Ali Marjaninejad, Bruce McNaughton, Risto Miikkulainen, Zaneta Navratilova, Tej Pandit, Alice Parker, Praveen K. Pilly, Sebastian Risi, Terrence J. Sejnowski, Andrea Soltoggio, Nicholas Soares, Andreas S. Tolias, Darío Urbina-Meléndez, Francisco J. Valero-Cuevas, Guido M. van de Ven, Joshua T. Vogelstein, Felix Wang, Ron Weiss, Angel Yanguas-Gil, Xinyun Zou, and Hava Siegelmann. Biological underpinnings for lifelong learning machines. *Nature Machine Intelligence* 2022 4:3, 4(3):196–210, 2022. 1
- [13] Yan-Shuo Liang and Wu-Jun Li. Adaptive plasticity improvement for continual learning. In *2023 IEEE/CVF Conference on Computer Vision and Pattern Recognition (CVPR)*, pages 7816–7825, 2023. 6
- [14] Sen Lin, Li Yang, Deliang Fan, and Junshan Zhang. TRGP: Trust Region Gradient Projection for Continual Learning. *International Conference on Learning Representations*, 2022. 1, 3, 5, 6, 7, 8, 2
- [15] Sen Lin, Li Yang, Deliang Fan, and Junshan Zhang. Beyond not-forgetting: continual learning with backward knowledge transfer. In *Proceedings of the 36th International Conference on Neural Information Processing Systems*, Red Hook, NY, USA, 2022. Curran Associates Inc. 1, 3, 6, 8
- [16] David Lopez-Paz and Marc ' Aurelio Ranzato. Gradient Episodic Memory for Continual Learning. In *Proceedings of the 31st International Conference on Neural Information Processing Systems*, 2017. 1, 3, 5, 2
- [17] Arun Mallya and Svetlana Lazebnik. PackNet: Adding Multiple Tasks to a Single Network by Iterative Pruning. *2018 IEEE/CVF Conference on Computer Vision and Pattern Recognition*, pages 7765–7773, 2017. 1, 3
- [18] Qi Qin, Wenpeng Hu, Han Peng, Dongyan Zhao, and Bing Liu. BNS: Building Network Structures Dynamically for Continual Learning. *Advances in Neural Information Processing Systems*, 34:20608–20620, 2021. 1, 3
- [19] Sylvestre Alvisé Rebuffi, Alexander Kolesnikov, Georg Sperl, and Christoph H. Lampert. iCaRL: Incremental Classifier and Representation Learning. *2017 IEEE Conference on Computer Vision and Pattern Recognition (CVPR)*, 2017-January:5533–5542, 2017. 1, 3
- [20] H. Ritter, Aleksandar Botev, and D. Barber. Online Structured Laplace Approximations For Overcoming Catastrophic Forgetting. *Neural Information Processing Systems*, 2018. 3
- [21] Andrei A. Rusu, Neil C. Rabinowitz, Guillaume Desjardins, Hubert Soyer, James Kirkpatrick, Koray Kavukcuoglu, Razvan Pascanu, and Raia Hadsell. Progressive Neural Networks. *arXiv preprint arXiv:1606.04671*, 2016. 1, 3
- [22] Gobinda Saha and Kaushik Roy. Continual Learning with Scaled Gradient Projection. *Proceedings of the 37th AAAI Conference on Artificial Intelligence, AAAI 2023*, 37:9677–9685, 2023. 1, 2, 3, 5, 6, 8

- [23] Gobinda Saha, Isha Garg, and K. Roy. Gradient Projection Memory for Continual Learning. *International Conference on Learning Representations*, 2021. 1, 2, 3, 5, 6, 8
- [24] Jonathan Schwarz, Wojciech M. Czarnecki, Jelena Luketina, A. Grabska-Barwinska, Y. Teh, Razvan Pascanu, and R. Hadsell. Progress & Compress: A scalable framework for continual learning. *International Conference on Machine Learning*, 2018. 3
- [25] J. Serrà, Dídac Surís, M. Miron, and Alexandros Karatzoglou. Overcoming catastrophic forgetting with hard attention to the task. *International Conference on Machine Learning*, 2018. 1, 3, 6, 2
- [26] Yujun Shi, Li Yuan, Yunpeng Chen, and Jiashi Feng. Continual Learning via Bit-Level Information Preserving. *2021 IEEE/CVF Conference on Computer Vision and Pattern Recognition (CVPR)*, pages 16669–16678, 2021. 1
- [27] O. Vinyals, C. Blundell, T. Lillicrap, K. Kavukcuoglu, and Daan Wierstra. Matching Networks for One Shot Learning. *Neural Information Processing Systems*, 2016. 5
- [28] Liyuan Wang, Xingxing Zhang, Hang Su, and Jun Zhu. A Comprehensive Survey of Continual Learning: Theory, Method and Application. *IEEE Transactions on Pattern Analysis and Machine Intelligence*, 46(08):5362–5383, 2024. 1, 3, 4
- [29] Shipeng Wang, Xiaorong Li, Jian Sun, and Zongben Xu. Training Networks in Null Space of Feature Covariance for Continual Learning. *2021 IEEE/CVF Conference on Computer Vision and Pattern Recognition (CVPR)*, pages 184–193, 2021. 1
- [30] Ju Xu and Zhanxing Zhu. Reinforced Continual Learning. In *Proceedings of the 32nd International Conference on Neural Information Processing Systems*, pages 907–916, 2018. 1, 3
- [31] Enneng Yang, Li Shen, Zhenyi Wang, Shiwei Liu, Guibing Guo, and Xingwei Wang. Data augmented flatness-aware gradient projection for continual learning. In *2023 IEEE/CVF International Conference on Computer Vision (ICCV)*, pages 5607–5616, 2023. 3, 6
- [32] Jaehong Yoon, Eunho Yang, Jeongtae Lee, and Sung Ju Hwang. Lifelong Learning with Dynamically Expandable Networks. *International Conference on Learning Representations*, 2018. 1, 3
- [33] Jaehong Yoon, Saehoon Kim, Eunho Yang, and Sung Ju Hwang. Scalable and Order-robust Continual Learning with Additive Parameter Decomposition. *International Conference on Learning Representations*, 2020. 1
- [34] Guanxiong Zeng, Yang Chen, Bo Cui, and Shan Yu. Continual learning of context-dependent processing in neural networks. *Nature Machine Intelligence* 2019 1:8, 1(8):364–372, 2019. 1, 3, 6
- [35] Friedemann Zenke, Ben Poole, and Surya Ganguli. Continual Learning Through Synaptic Intelligence. *Proceedings of machine learning research*, 70:3987, 2017. 1, 3
- [36] Chiyuan Zhang, Samy Bengio, Moritz Hardt, Benjamin Recht, and Oriol Vinyals. Understanding deep learning requires rethinking generalization. In *International Conference on Learning Representations*, 2017. 2, 3
- [37] Zhen Zhao, Zhizhong Zhang, Xin Tan, Jun Liu, Yanyun Qu, Yuan Xie, and Lizhuang Ma. Rethinking gradient projection continual learning: Stability/plasticity feature space decoupling. In *2023 IEEE/CVF Conference on Computer Vision and Pattern Recognition (CVPR)*, pages 3718–3727, 2023. 3, 6

# CODE-CL: Conceptor-Based Gradient Projection for Deep Continual Learning

## Supplementary Material

### A. Conceptor Implementation Details

We implement the conceptor operations following the equations presented in Section 2, with one exception: the AND operation (4).

The operation defined in (4) is only valid when the conceptor matrices are invertible. However, in practice, since we use a limited number of samples to compute the conceptors, the resulting matrices are often not full rank. To address this, we adopt a more general version of the AND operation, as proposed in [8]:

$$C \wedge B = D(D^\top(C^\dagger + B^\dagger - I)D)^{-1}D^\top, \quad (11)$$

Here,  $C^\dagger$  and  $B^\dagger$  denote the pseudo-inverses of  $C$  and  $B$ , respectively. The matrix  $D$  consists of columns that form an arbitrary orthonormal basis for the intersection of the column spaces of  $C$  and  $B$ .

The procedure for computing  $D$  is outlined in Algorithm 2.

---

#### Algorithm 2 Computation of matrix $D$ in (11)

---

**Input:**  $C, B, \beta$  (threshold),  $N$  (dimension of  $C$  and  $B$ )

**Output:**  $D$

```

 $U_C, S_C \leftarrow \text{SVD}(C)$     ▷ Singular value decomposition
 $U_B, S_B \leftarrow \text{SVD}(B)$ 
 $k_C \leftarrow \text{num\_elements}(S_C > \beta)$     ▷ # of elements  $> \beta$ 
 $k_B \leftarrow \text{num\_elements}(S_B > \beta)$ 
 $U'_C \leftarrow U_C[:, k_C :]$     ▷ Last  $N - k_C$  columns
 $U'_B \leftarrow U_B[:, k_B :]$ 
 $U, S \leftarrow \text{SVD}(U'_C U'^{\top}_C + U'_B U'^{\top}_B)$ 
 $k \leftarrow \text{num\_elements}(S > \beta)$ 
 $D \leftarrow U[:, k :]$ 

```

---

### B. Additional Ablation Studies

In this section, we present additional ablation studies to evaluate the impact of the number of free dimensions ( $K$ ) and aperture ( $\alpha$ ) on the 5-Datasets benchmark, as well as the effect of the threshold parameter ( $\epsilon$ ) across all three benchmarks.

Tables 5 and 6 summarize the results on the 5-Datasets benchmark. We observe that increasing  $\alpha$  leads to a reduction in BWT, consistent with the findings in Section 4. Similarly, increasing  $K$  improves final accuracy, further validating trends observed in the other datasets.

Regarding the threshold parameter ( $\epsilon$ ), results suggest that lower values of  $\epsilon$  enhance performance by allowing more directions in the intersection of input spaces across

Table 5. Ablation studies on the aperture ( $\alpha$ ) hyperparameter on the 5-Datasets benchmark. Results are reported as mean  $\pm$  standard deviation over five trials. Other hyperparameters are constant as reported in Section 4.

$\alpha$	ACC (%)	BWT (%)
4	93.32 $\pm$ 0.13	-0.25 $\pm$ 0.02
8	<b>93.51 <math>\pm</math> 0.13</b>	-0.11 $\pm$ 0.01
16	93.46 $\pm$ 0.16	-0.04 $\pm$ 0.00

Table 6. Ablation studies on the number of free dimensions ( $K$ ) parameter on the 5-Datasets benchmark. Results are reported as mean  $\pm$  standard deviation over five trials. Other hyperparameters are constant as reported in Section 4.

$K$	ACC (%)	BWT (%)
0	91.67 $\pm$ 0.31	-1.36 $\pm$ 0.07
20	92.70 $\pm$ 0.07	-0.43 $\pm$ 0.01
40	93.08 $\pm$ 0.08	-0.33 $\pm$ 0.09
60	93.22 $\pm$ 0.16	-0.28 $\pm$ 0.00
80	<b>93.32 <math>\pm</math> 0.13</b>	-0.25 $\pm$ 0.00

Table 7. Ablation studies on the threshold ( $\epsilon$ ) across the four benchmarks. Results are reported as mean  $\pm$  standard deviation over five trials. Other hyperparameters are constant as reported in Section 4.

	$\epsilon$	ACC (%)	BWT (%)
S-CIFAR100	0.2	<b>77.51 <math>\pm</math> 0.18</b>	-0.84 $\pm$ 0.24
	0.5	77.21 $\pm$ 0.32	-1.10 $\pm$ 0.28
	0.8	75.71 $\pm$ 0.40	-0.93 $\pm$ 0.36
S-MiniImageNet	0.2	68.61 $\pm$ 0.94	-1.30 $\pm$ 0.18
	0.5	<b>68.83 <math>\pm</math> 0.41</b>	-1.10 $\pm$ 0.30
	0.8	66.57 $\pm$ 0.24	-0.56 $\pm$ 0.18
5-Datasets	0.2	<b>93.42 <math>\pm</math> 0.11</b>	-0.20 $\pm$ 0.06
	0.5	93.32 $\pm$ 0.13	-0.25 $\pm$ 0.02
	0.8	92.28 $\pm$ 0.24	-0.71 $\pm$ 0.18

tasks to be freed. However, this also increases memory requirements. Therefore, selecting an appropriate  $\epsilon$  involves a trade-off between performance and computational resources.

### C. Experimental Setup

This section provides details on the architecture of all models used in this work, the dataset statistics, the hyperparameters for each experiment, and the compute resources employed.

Table 8. 5-Datasets statistics.

Dataset	CIFAR10	MNIST	SVHN	Fashion MNIST	notMNIST
Number of classes	10	10	10	10	10
Training samples	47500	57000	69595	57000	16011
Validation samples	2500	3000	3662	3000	842
Test samples	10000	10000	26032	10000	1873

Table 9. List of hyperparameters used in our experiments.

Dataset	Split CIFAR100	Split miniImageNet	5-Datasets
Learning rate ( $\eta$ )	0.01	0.1	0.1
Batch size ( $b$ )	64	64	64
Batch size for conceptor comp. ( $b_s$ )	125	125	125
Min. learning rate ( $\eta_{th}$ )	$10^{-5}$	$10^{-5}$	$10^{-3}$
Learning rate decay factor	1/2	1/2	1/3
Patience	6	6	5
Number of epochs ( $E$ )	200	100	100
Aperture ( $\alpha$ )	6	8	4
Threshold ( $\epsilon$ )	0.5	0.5	0.5

Table 10. Split CIFAR100 and Split miniImageNet datasets statistics.

Dataset	Split CIFAR100	Split miniImageNet
Number of tasks ( $T$ )	10	20
Sample dimensions	$3 \times 32 \times 32$	$3 \times 84 \times 84$
Number of classes per task	10	5
Training samples per task	4750	2375
Validation samples per task	250	125
Test samples per task	1000	500

### C.1. Model Architecture

In this work, we utilize two models: an AlexNet-like architecture, as described in [25], and a Reduced ResNet18 [16].

The AlexNet-like model incorporates batch normalization (BN) in every layer except the classifier layer. The BN layers are trained during the first task and remain frozen for subsequent tasks. The model consists of three convolutional layers with 64, 128, and 256 filters, using kernel sizes of  $4 \times 4$ ,  $3 \times 3$ , and  $2 \times 2$ , respectively. These are followed by two fully connected layers, each containing 2048 neurons. ReLU activation functions are used throughout, along with  $2 \times 2$  max-pooling layers after each convolutional layer. Dropout is applied with rates of 0.2 for the first two layers and 0.5 for the remaining layers.

The Reduced ResNet18 follows the architecture detailed in [23]. For the Split miniImageNet experiments, the first layer uses a stride of 2, while for the 5-Datasets benchmark, it uses a stride of 1.

For all models and experiments, cross-entropy loss is employed as the loss function.

### C.2. Dataset Statistics

The statistics for the four benchmarks used in this work for continual image classification are summarized in Table 10 and Table 8. For all benchmarks, we follow the same data partitions as those used in [14, 22, 23].

For the 5-Datasets benchmark, grayscale images are replicated across all RGB channels to ensure compatibility with the architecture. Additionally, all images are resized to  $32 \times 32$  pixels, resulting in an input size of  $3 \times 32 \times 32$  for this benchmark.

### C.3. Hyperparameters

The hyperparameters used in our experiments are detailed in Table 9.

### C.4. Compute resources

All experiments were conducted on a shared internal Linux server equipped with an AMD EPYC 7502 32-Core Processor, 504 GB of RAM, and four NVIDIA A40 GPUs, each with 48 GB of GDDR6 memory. Additionally, code was implemented using Python 3.9 and PyTorch 2.2.1 with CUDA 11.8.